Systematic study of near-yrast band structures in odd-mass $^{125-137}$Pr and $^{127-139}$Pm isotopes

S. Jehangir,[1] G. H. Bhat,[2,3,4] N. Rather,[1] J. A. Sheikh,[4] and R. Palit[5]

[1]*Department of Physics, Islamic University of Science and Technology, Jammu and Kashmir 192 122, India*
[2]*Department of Physics, S.P. College, Srinagar, Jammu and Kashmir 190001, India*
[3]*Cluster University Srinagar, Jammu and Kashmir, Srinagar, Goji Bagh 190008, India*
[4]*Department of Physics, University of Kashmir, Hazratbal, Srinagar 190006, India*
[5]*Department of Nuclear and Atomic Physics, Tata Institute of Fundamental Research, Mumbai-400005, India*

(Received 3 June 2021; accepted 6 October 2021; published 20 October 2021)

In the present work, the basis space in the triaxial projected shell-model approach is expanded to include three and five quasiparticle configurations for odd-proton systems. This extension allows us to investigate the high-spin band structures observed in odd-proton systems up to and including the second band-crossing region and, as a first major application of this development, the high-spin properties are investigated for odd-mass $^{125-137}$Pr and $^{127-139}$Pm isotopes. It is shown that band crossings in the studied isotopes have mixed structures with the first crossing dominated by one-proton coupled to two-neutron configuration for the lighter isotopes which then changes to three-proton configuration with increasing neutron number. Furthermore, γ bands based on quasiparticle states are also delineated in the present work, and it is predicted that these band structures built on three-quasiparticle configurations become favored in energy for heavier systems in the high-spin region.

DOI: 10.1103/PhysRevC.104.044322

I. INTRODUCTION

Nuclei in the mass ≈130 region are known to exhibit a rich variety of shapes and structures. In this region, interesting phenomena of shape coexistence [1,2], strongly deformed [3] to superdeformed [4,5] shapes, chiral doublet bands [6,7], and γ bands built on quasiparticle states [8–10] have been observed. This is the heaviest mass region with valence neutrons and protons occupying the same intruder orbital, $1h_{11/2}$. For the neutron-deficient isotopic chains in this mass region, protons occupy the low-Ω orbitals, whereas neutron occupancy changes from mid-Ω to high-Ω orbitals of $1h_{11/2}$. Due to the competing shape polarizing effects of low-Ω and high-Ω orbitals, the neutron-deficient nuclei in this region are expected to have, in general, triaxial shapes [11,12].

The interplay between proton and neutron configurations also plays an important role in the elucidation of the high-spin band structures observed in this mass region. Band structures have been observed up to quite high spin, and band-crossing features have attracted considerable attention [13–15]. In particular, the nature of the band crossings in odd-proton Pr and Pm isotopes has been extensively studied in recent years [16–20]. It has been shown that the standard cranked shell-model (CSM) approach with fixed pairing and deformation fields can describe the band-crossing features reasonably well for heavier Pr and Pm isotopes. However, for lighter isotopes of ^{127}Pr and ^{131}Pm, the gain in alignment is substantially underpredicted using this approach [21]. The band crossings in these nuclei have also been investigated using the extended version of total Routhian surface (TRS) approach [21], in which pairing and deformation fields are determined self-consistently. The observed band crossing features have been reproduced in this more realistic approach, and it has been demonstrated that the nature of the first band crossing is quite different from that predicted using the standard CSM approach. It has been shown that, for lighter isotopes, band crossings for these isotopes have a dominant contribution from the neutron configuration. This is in contradiction with the standard CSM results which predict proton BC crossing earlier than the neutron AB crossing for these nuclei.

Furthermore, band-crossing features in odd-proton isotopes have been investigated using the projected shell model (PSM) approach. In this model, basis states are constructed from the solutions of the Nilsson potential with axial symmetry [22]. In the study of odd-proton nuclei, the basis space in PSM is comprised of one-proton and one-proton coupled to two-neutron configurations. It has been shown using this approach that band crossing features of lighter isotopes of promethium could be described well. However, for heavier isotopes, discrepancies were observed between the PSM prediction and the experimental data. The major reason for this discrepancy is due to neglect of the proton aligning configurations in the basis space of PSM since it is evident from the CSM analysis [21] that the proton contribution becomes more dominant for heavier Pr and Pm isotopes. To elucidate the band crossing features for these isotopes, it is imperative to include both neutron- and proton-aligning configurations in the basis space. In the present work, we have generalized the basis space of the projected shell model for odd-proton systems by including proton aligning configurations in addition to the neutron states. The generalized basis configuration space has been implemented in the three-dimensional version

TABLE I. Axial and triaxial quadrupole deformation parameters ε and ε' employed in the TPSM calculation.

	^{125}Pr	^{127}Pr	^{129}Pr	^{131}Pr	^{133}Pr	^{135}Pr	^{137}Pr	^{127}Pm	^{129}Pm	^{131}Pm	^{133}Pm	^{135}Pm	^{137}Pm	^{139}Pm
ε	0.300	0.283	0.267	0.234	0.194	0.150	0.150	0.300	0.300	0.300	0.292	0.230	0.200	0.190
ε'	0.100	0.100	0.100	0.101	0.090	0.080	0.080	0.110	0.110	0.110	0.120	0.110	0.100	0.090
γ	18.4	19.5	20.5	23.3	24.8	28.1	28.1	20.1	20.1	20.1	22.3	25.6	26.5	25.3

of the projected shell model, what is now referred to as the triaxial projected shell model (TPSM) as most of the Pr and Pm isotopes discussed in the present work are predicted to have triaxial shapes. Five-quasiparticle configurations have also been included in the basis space, which allows us to investigate the second band crossing observed in some of these isotopes.

It needs to be mentioned that, during the development of the present generalized TPSM approach for odd-proton systems, new experimental data on high-spin states in ^{135}Pm became available and preliminary TPSM results for this particular system were published in Ref. [16] with the experimental group. In the present study, we have performed a detailed study using the generalized TPSM approach for fourteen Pr and Pm isotopes. We would also like to add that the PSM approach has recently been generalized to include higher quasiparticle configurations using the Pfaffian algebra [23–25]. In the present work, we have

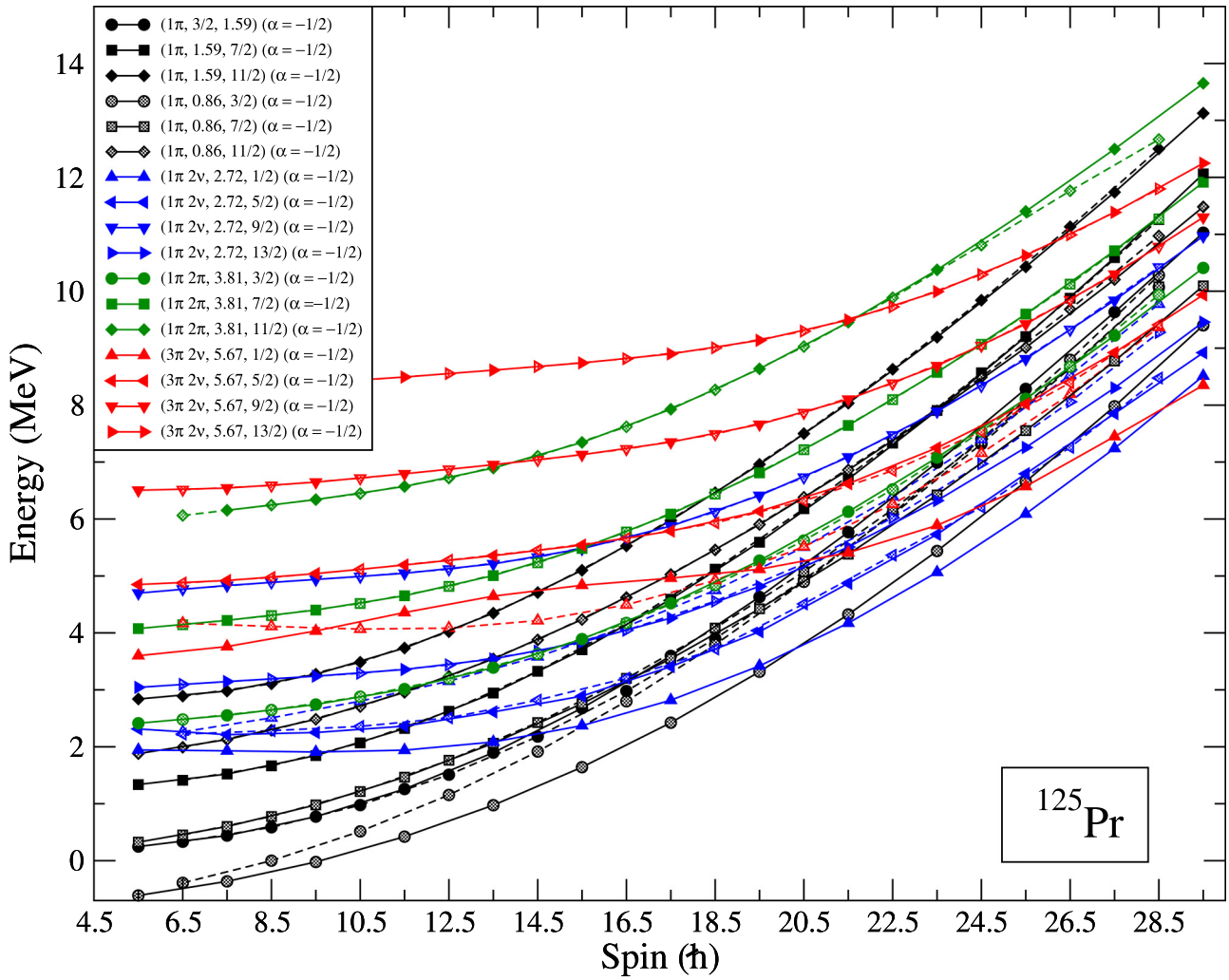

FIG. 1. Projected energies are shown before diagonalization of the shell-model Hamiltonian for ^{125}Pr. The bands are labeled by three quantities: group structure, energy and K quantum number of the quasiparticle state. For instance, $(1\pi, 1.54, 3/2)$ designates a one-quasiproton state having an intrinsic energy of 1.54 MeV and $K = 3/2$. The two signature bands for low-K states are depicted separately because the energy splitting between the two branches is large and the plots become quite clumsy when plotted as a single curve. In the legend of the figure, bands are designated for $\alpha = -1/2$ states and for the $\alpha = +1/2$ states the same symbols are used except that the corresponding curves are dashed lines.

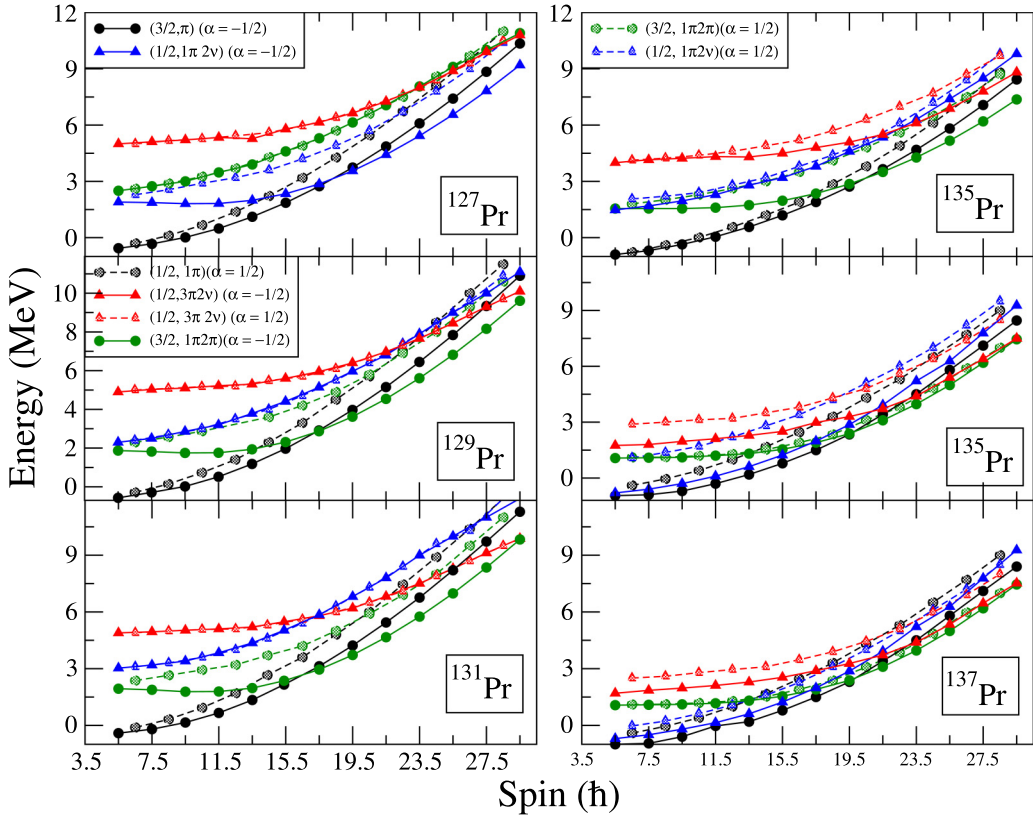

FIG. 2. Band diagrams for odd-proton $^{127-137}$Pr isotopes. The bands are labeled as in Fig. 1 with solid lines representing $\alpha = -1/2$ and the dashed curves designating $\alpha = +1/2$. Only the potions of diagrams that encompasses the band crossing are displayed.

employed the generalized Wick's theorem to evaluate the norm and energy kernels, which become quite tedious for multiquasiparticle configurations. In the future, we are planning to evaluate the kernels using the simpler Pfaffian approach.

In recent years, the TPSM approach has turned out to be a useful tool to investigate the high-spin band structures in deformed and transitional nuclei [26–29]. The model has provided some new insights into the nature of the high-spin band structures in even-even and odd-odd nuclei in the mass ≈130 region. The chiral doublet bands observed in this mass region have been well described using the TPSM approach [26,30]. For a few even-even Ce- and Nd-isotopes, it has been demonstrated that some excited band structures observed are γ bands built on two-quasiparticle states [31]. There has been an anomaly in the g-factor measurements for the bandheads of the s bands observed in these nuclei [32–37]. The g factors for the two observed s bands are either positive or negative, implying that the character of both the s bands is either proton or neutron. In the mass ≈130 region, the Fermi surfaces of neutrons and protons are close in energy and it is, therefore, expected that neutrons and protons will align almost simultaneously. From this perspective, it is expected that two observed s bands should have neutron and proton structures, respectively. The corresponding g factors should be positive and negative for the two s bands. The observation of both s bands having positive or negative g factors is ruled out using this standard picture.

It has been shown using the TPSM approach that each quasiparticle state has a γ band built on it [43] and the second excited s band, as a matter of fact, is a γ band built on the two-quasiparticle state. As the intrinsic structures of the two-quasiparticle band and the γ band built on it is same, the predicted g factors for two bands should be similar. This explained why both the observed s bands have either positive or negative g-factor values [32,37].

As cerium and neodymium are even-even cores of odd-mass praseodymium and promethium nuclei, it is expected that these odd-mass nuclei should also depict γ bands built on quasiparticle states. γ bands in some odd-mass nuclei have already been identified [44]. To delineate γ bands in high-spin band structures of odd-mass Pr and Pm isotopes is one of the objectives of the present work. The paper is organized in the following manner: In the next section, the extended TPSM approach is briefly presented. In Sec. III, TPSM results obtained for Pr and Pm isotopes are compared with the experimental data, where ever available. Finally, the summary and conclusions obtained in the present study are outlined in Sec. IV.

II. TRIAXIAL PROJECTED SHELL-MODEL APPROACH

The inclusion of multiquasiparticle basis space in TPSM approach has made it feasible to study not only the ground-state properties but also the high-spin band structures in deformed and transitional nuclei [37,43,45]. Using the TPSM

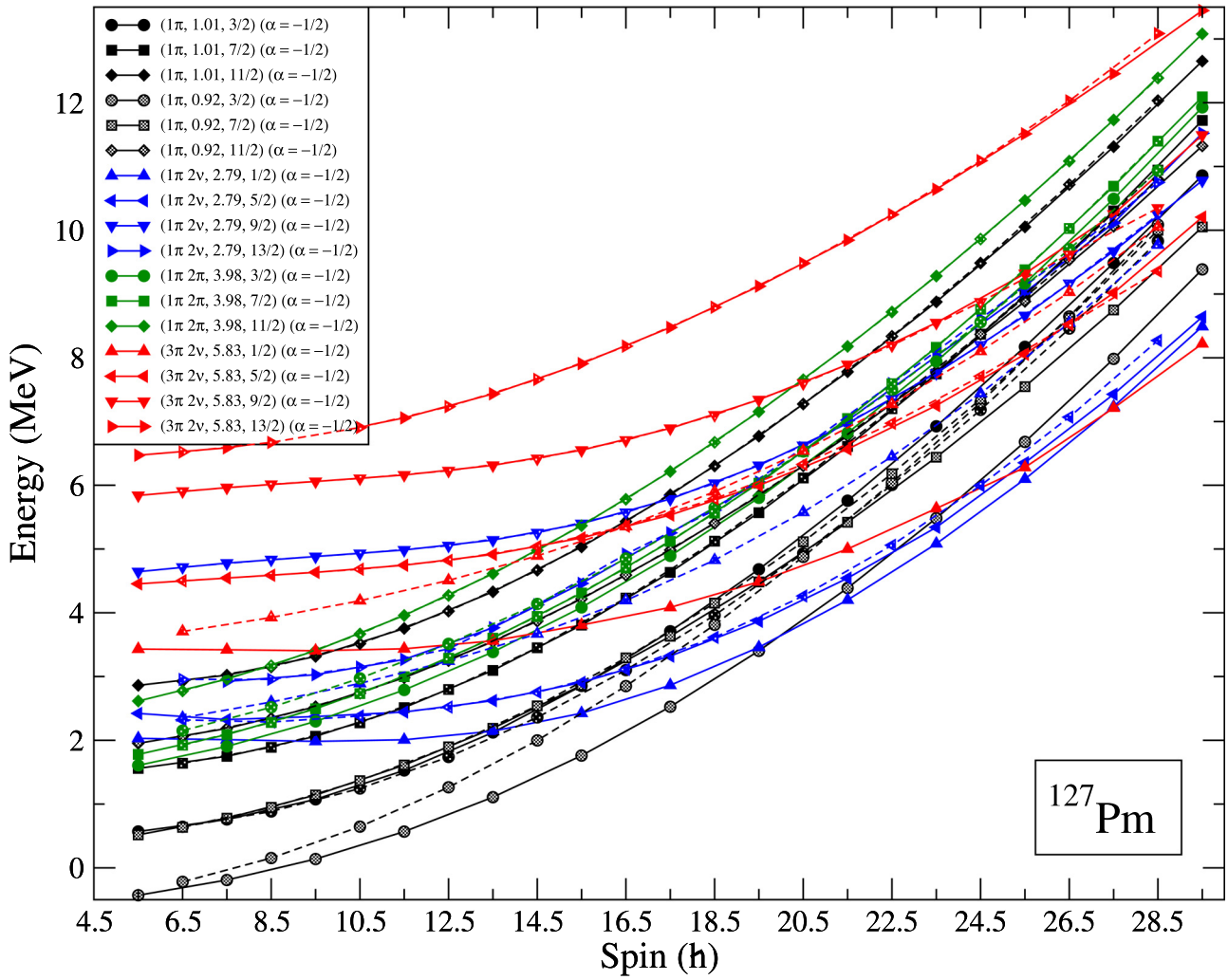

FIG. 3. Projected energies before diagonalization are shown for ^{127}Pm. The labeling of the bands follows the Fig. 1 description.

approach, odd-proton systems have been studied earlier with the model space of one-proton and one-proton coupled to two-neutron quasiparticle states. However, in order to investigate the high-spin spectroscopy of these systems, the basis space needs to be extended by including proton aligning configurations, in addition to the neutron states. In the present work, the extended basis space has been implemented and the complete basis space in the generalized approach is given by

$$\begin{aligned}
&\hat{P}^I_{MK} a^\dagger_{\pi_1} |\Phi\rangle, \\
&\hat{P}^I_{MK} a^\dagger_{\pi_1} a^\dagger_{\nu_1} a^\dagger_{\nu_2} |\Phi\rangle, \\
&\hat{P}^I_{MK} a^\dagger_{\pi_1} a^\dagger_{\pi_2} a^\dagger_{\pi_3} |\Phi\rangle, \\
&\hat{P}^I_{MK} a^\dagger_{\pi_1} a^\dagger_{\pi_2} a^\dagger_{\pi_3} a^\dagger_{\nu_1} a^\dagger_{\nu_2} |\Phi\rangle,
\end{aligned} \tag{1}$$

where $|\Phi\rangle$ is the triaxially deformed quasiparticle vacuum state. P^I_{MK} is the three-dimensional angular-momentum-projection operator given by [46]

$$\hat{P}^I_{MK} = \frac{2I+1}{8\pi^2} \int d\Omega D^I_{MK}(\Omega) \hat{R}(\Omega), \tag{2}$$

with the rotation operator

$$\hat{R}(\Omega) = e^{-i\alpha \hat{J}_z} e^{-i\beta \hat{J}_y} e^{-i\gamma \hat{J}_z}. \tag{3}$$

Here, "Ω" represents the set of Euler angles ($\alpha, \gamma = [0, 2\pi]$, $\beta = [0, \pi]$) and $\hat{J}_y$ and $\hat{J}_z$ are the angular-momentum operators. The angular-momentum projection operator in Eq. (2) not only projects out the good angular momentum but also states having good K values by specifying a value for K in the rotational matrix D in Eq. (2).

The constructed projected basis of Eq. (1) is then used to diagonalize the shell-model Hamiltonian, consisting of the harmonic-oscillator single-particle Hamiltonian and a residual two-body interaction comprising of quadrupole-quadrupole, monopole pairing, and quadrupole pairing terms. These terms represent specific correlations which are considered to be essential to describe the low-energy nuclear phenomena [47]. The Hamiltonian has the following form:

$$\hat{H} = \hat{H}_0 - \frac{1}{2}\chi \sum_\mu \hat{Q}^\dagger_\mu \hat{Q}_\mu - G_M \hat{P}^\dagger \hat{P} - G_Q \sum_\mu \hat{P}^\dagger_\mu \hat{P}_\mu. \tag{4}$$

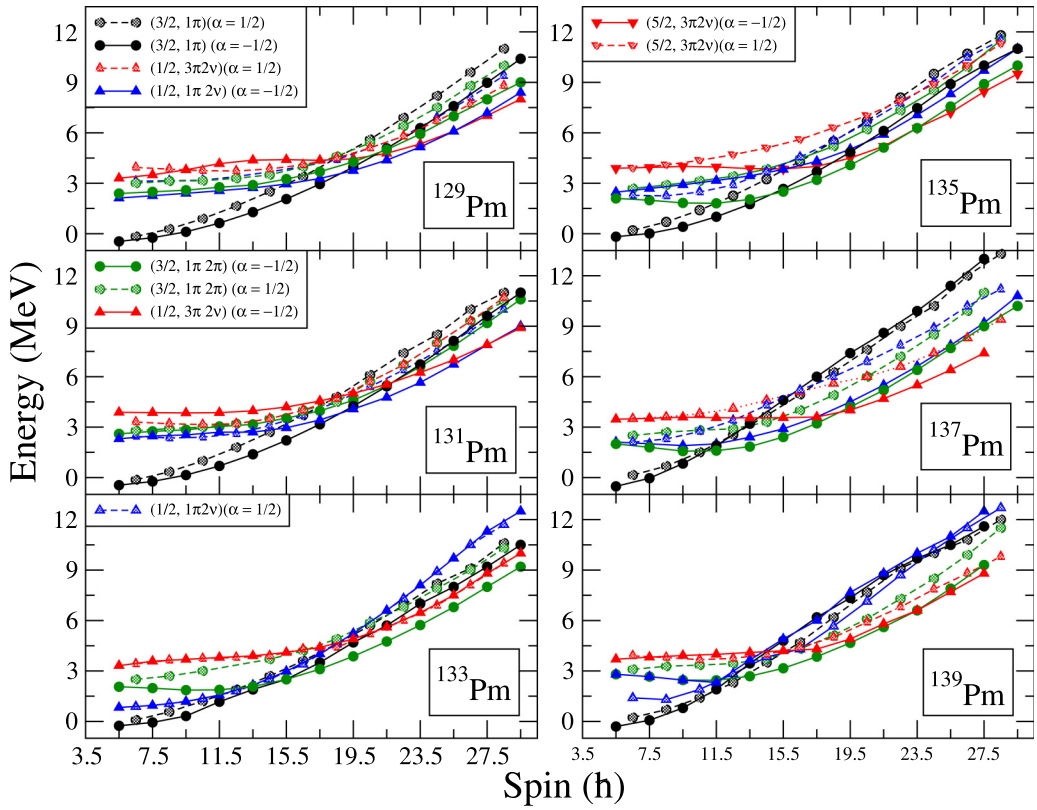

FIG. 4. Band diagrams for $^{129-139}$Pm isotopes. The figure is similar to Fig. 2.

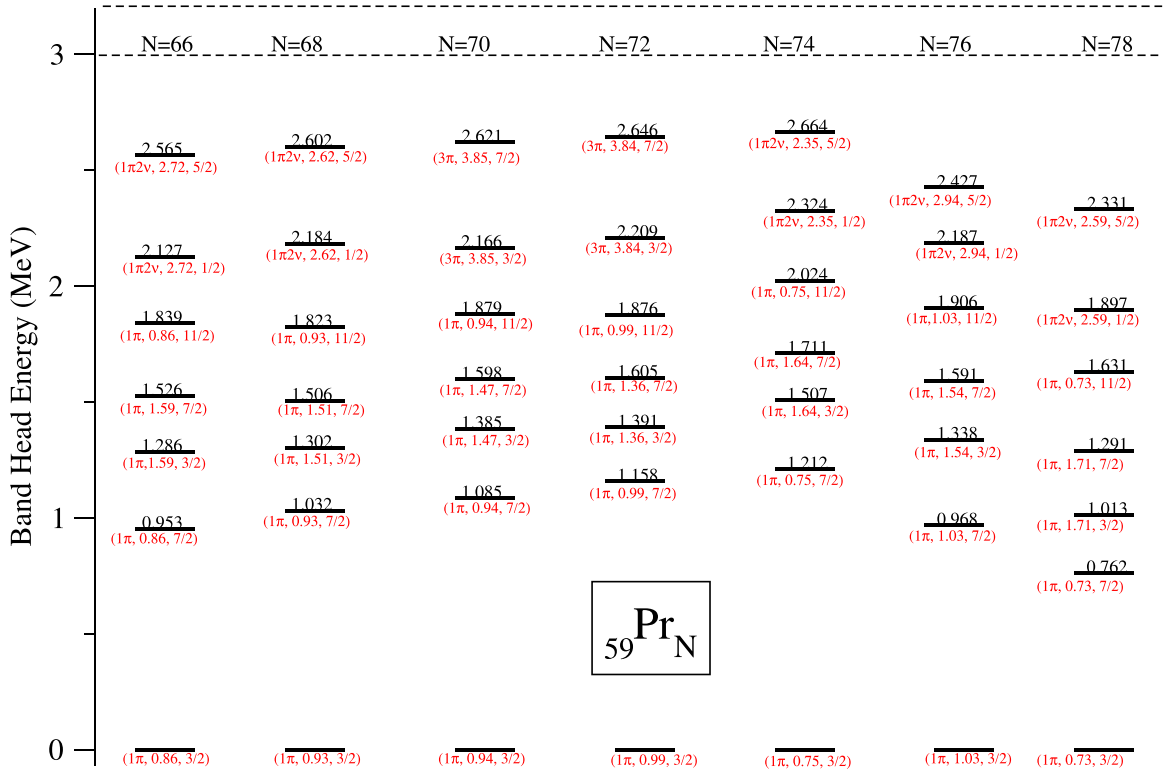

FIG. 5. TPSM bandhead energies after configuration mixing for odd-proton $^{125-137}$Pr isotopes. The dominant intrinsic configuration is specified for each state.

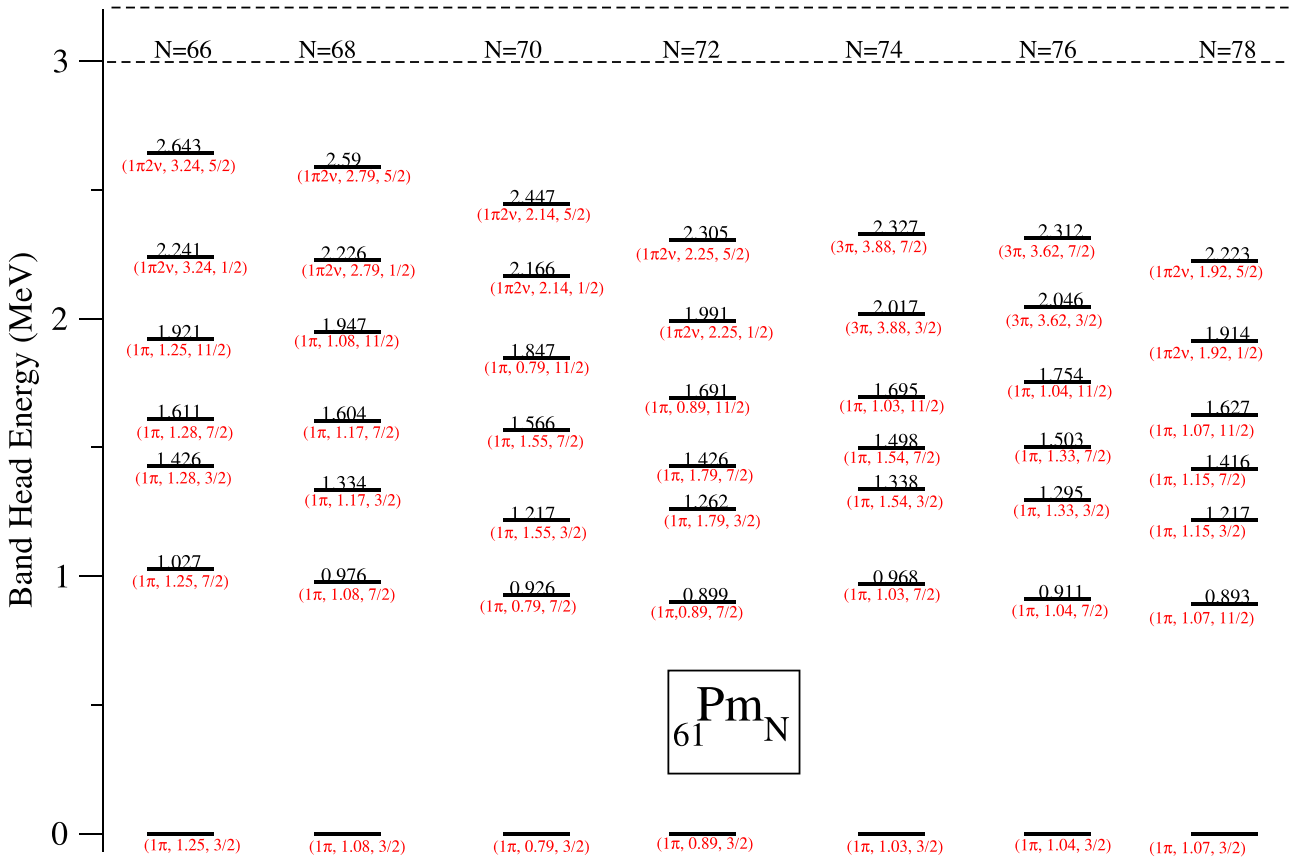

FIG. 6. TPSM bandhead energies after configuration mixing for odd-proton $^{127-139}$Pm isotopes. The dominant intrinsic configuration is specified for each state.

In the above equation, $\hat{H}_0$ is the spherical single-particle part of the Nilsson potential [48]. The QQ-force strength χ in Eq. (4) is related to the quadrupole deformation ϵ as a result of the self-consistent Hartree-Fock-Bogolyubov (HFB) condition and the relation is given by [49]

$$\chi_{\tau\tau'} = \frac{\frac{2}{3}\epsilon\hbar\omega_\tau\hbar\omega_{\tau'}}{\hbar\omega_n\langle\hat{Q}_0\rangle_n + \hbar\omega_p\langle\hat{Q}_0\rangle_p}, \tag{5}$$

where $\omega_\tau = \omega_0 a_\tau$, with $\hbar\omega_0 = 41.4678A^{-\frac{1}{3}}$ MeV, and the isospin-dependence factor a_τ is defined as

$$a_\tau = \left[1 \pm \frac{N-Z}{A}\right]^{\frac{1}{3}},$$

with $+$ $(-)$ for $\tau =$ neutron (proton). The harmonic oscillation parameter is given by $b_\tau^2 = b_0^2/a_\tau$ with $b_0^2 = \hbar/(m\omega_0) = A^{\frac{1}{3}}$ fm^2. The monopole pairing strength G_M (in MeV) is of the standard form

$$G_M = \frac{G_1 \mp G_2\frac{N-Z}{A}}{A}, \tag{6}$$

where the minus (plus) sign applies to neutrons (protons). In the present calculation, we choose G_1 and G_2 such that the calculated gap parameters reproduce the experimental mass differences. This choice of G_M is appropriate for the single-particle space employed in the present calculation, where three major oscillator shells are used for each type of nucleons (N = 3, 4, 5 major shells for both neutrons and protons). The quadrupole pairing strength G_Q is assumed to be proportional to G_M, the proportionality constant being fixed as usual to be 0.16. These interaction strengths, although not exactly the same, are consistent with those used earlier in the TPSM calculations [26,30,44].

Using the angular-momentum projected states as the basis, the shell-model Hamiltonian of Eq. (4) is diagonalized following the Hill-Wheeler approach [49]. The generalized eigenvalue equation is given by

$$\sum_{\kappa'K'}\{\mathcal{H}^I_{\kappa K\kappa'K'} - E\mathcal{N}^I_{\kappa K\kappa'K'}\}f^I_{\kappa'K'} = 0, \tag{7}$$

where the Hamiltonian and norm kernels are given by

$$\mathcal{H}^I_{\kappa K\kappa'K'} = \langle\Phi_\kappa|\hat{H}\hat{P}^I_{KK'}|\Phi_{\kappa'}\rangle,$$
$$\mathcal{N}^I_{\kappa K\kappa'K'} = \langle\Phi_\kappa|\hat{P}^I_{KK'}|\Phi_{\kappa'}\rangle.$$

The Hill-Wheeler wave function is given by

$$|\psi_{IM}\rangle = \sum_{\kappa K} a^I_{\kappa K}\hat{P}^I_{MK}|\Phi_\kappa\rangle, \tag{8}$$

where $a^I_{\kappa K}$ are the variational coefficients, and the index κ designates the basis states of Eq. (1).

We would like to add that TPSM approach is quite similar in nature to that of the spherical shell-model approach, where

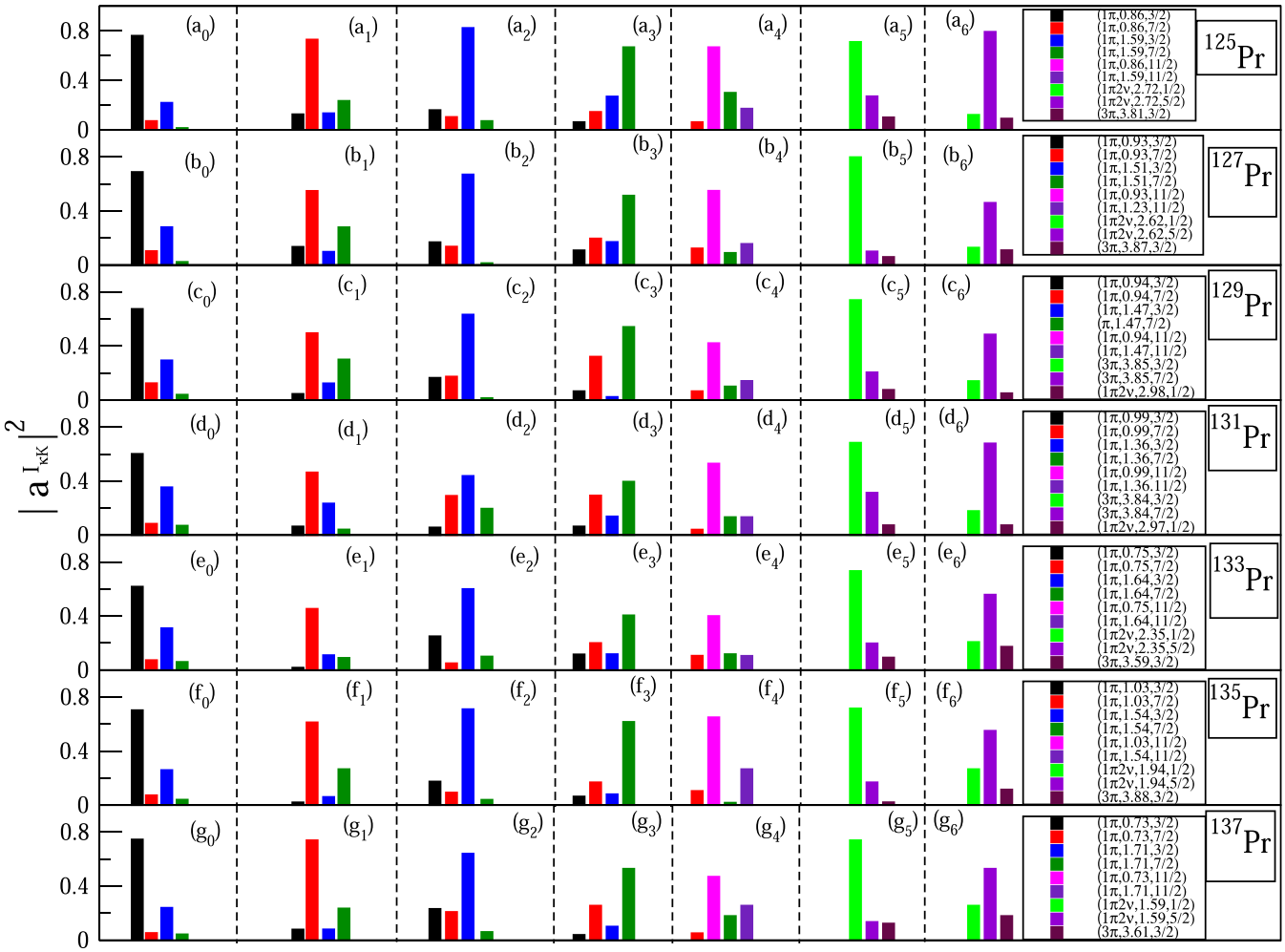

FIG. 7. Dominant probability contributions of various projected configurations in the wave functions of the bandhead structures shown in Fig. 5. The insets with labels a_0, a_1, a_2, a_3, a_4, a_5, and a_6 correspond to the ground-state, first, second, third, fourth, fifth, and sixth excited states of ^{125}Pr, respectively. The insets with label b, c, d, e, f, and g correspond to the ^{127}Pr, ^{129}Pr, ^{131}Pr, ^{133}Pr, ^{135}Pr, and ^{137}Pr isotopes, respectively.

the basis states are generated from the spherical mean-field potential. In the TPSM approach, the basis states are obtained from the deformed potential, which provides an optimum basis to study heavier deformed systems. The vacuum in the TPSM approach is generated by solving three-dimensional Nilsson potential, and then performing the BCS calculations. The multiquasiparticle states are then constructed by occupying the states in the intruder shell. These multiquasiparticle states are, in principle, expected to have somewhat reduced pairing content as compared with the vacuum state since some states are blocked. This reduced pairing for blocked states is disregarded in all the PSM and TPSM studies [43,49,50] as simplicity of the approach will be lost. To consider the pairing changes for the blocked states, it will be required to perform the BCS calculations of each quasiparticle state and then the mixing of these states needs to be performed using the more advanced approach of the generator coordinate method [46,51] because the mean-field for different quasiparticle states is different.

III. RESULTS AND DISCUSSION

TPSM calculations have been performed for odd-mass $^{125-137}$Pr and $^{127-139}$Pm isotopes using the axial and nonaxial deformations listed in Table I. These deformation values have been adopted from the earlier studies performed for these nuclei [16,22,52]. The intrinsic states obtained from the solution of the triaxial Nilsson potential with these deformation parameters are projected onto good angular-momentum states, as discussed in the previous section. For each system about 40 to 50 intrinsic states are selected around the Fermi surface for which the angular-momentum projection is performed. The angular-momentum-projected states, which are close to the yrast line, are depicted in Fig. 1 for ^{125}Pr. We would like to mention that all the projected states near the Fermi surface are employed in the final diagonalization of the shell-model Hamiltonian, but for clarity only projected states that are close to the yrast line are shown in Fig. 1. This diagram, what is referred to as the band diagram, is quite instructive because

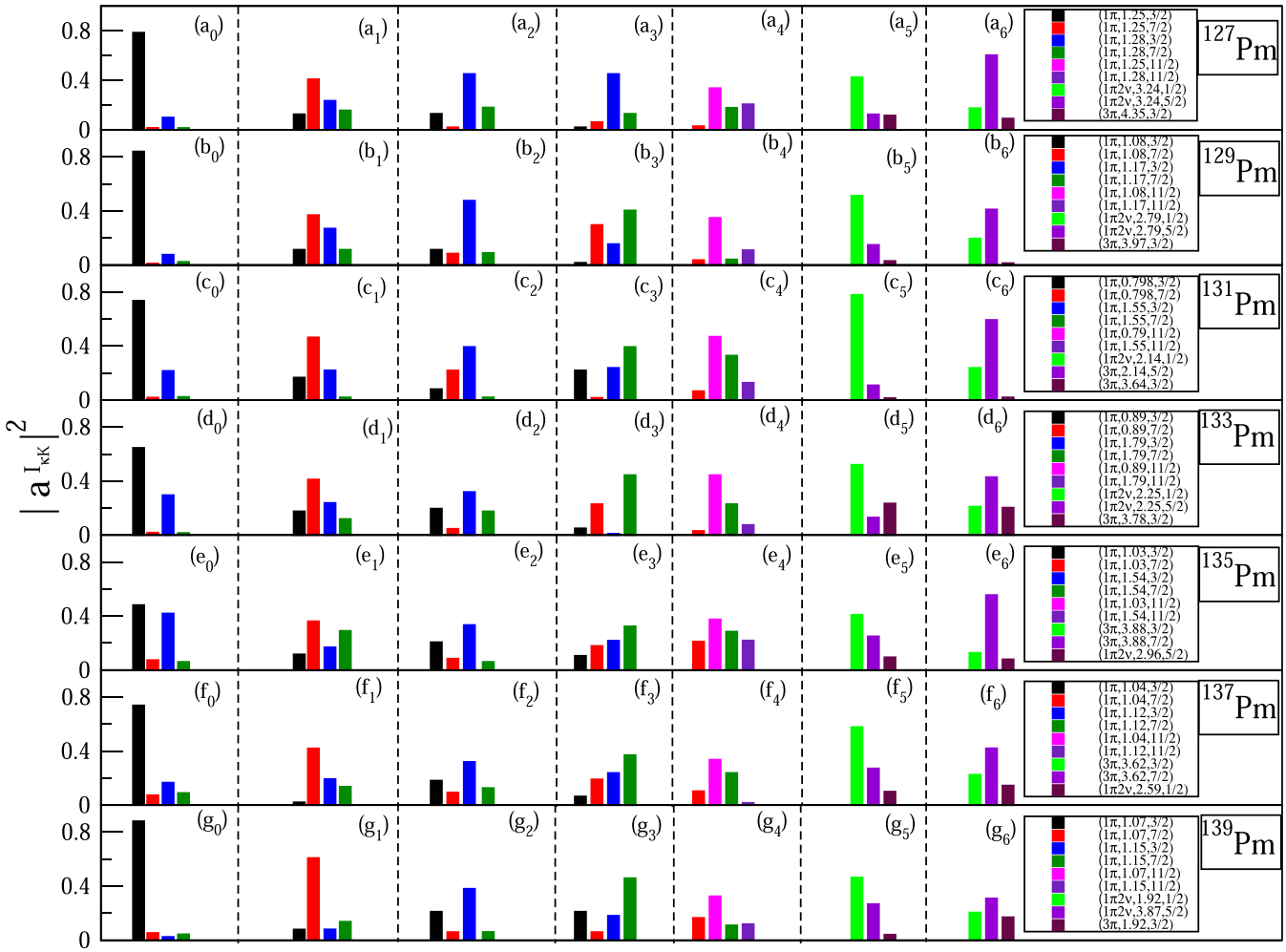

FIG. 8. Dominant probability contributions of various projected configurations in the wave functions of the bandhead structures shown in Fig. 6. The insets with labels a_0, a_1, a_2, a_3, a_4, a_5, and a_6 correspond to ground-state, first, second, third, fourth, fifth, and sixth excited states of ^{127}Pm. The insets with label b, c, d, e, f, and g correspond to the ^{129}Pm, ^{131}Pm, ^{133}Pm, ^{135}Pm, ^{137}Pm and ^{139}Pm isotopes, respectively.

it reveals the intrinsic structures of the observed band structures [49].

The lowest projected band in Fig. 1 originates from the one-quasiproton state, having $K = 3/2$, with the quasiparticle energy of 0.86 MeV. Although the triaxial quasiparticle state does not have a well-defined angular-momentum projection quantum number, the three-dimensional projection operator not only projects out the angular-momentum quantum number but also its projection along the intrinsic z axis, what is referred to as the K quantum number in the literature [53,54]. The K value specified in all the diagrams in the present work refers to this projected quantum number. The two signature branches for low-K bands are shown separately because the splitting between the two states is quite large for these configurations. The signature splitting for the lowest $K = 3/2$ band increases as expected with increasing angular momentum. It is noted from Fig. 1 that three-quasiparticle band comprised of one-proton and two-neutron aligned configuration, having $K = 1/2$, crosses the ground-state band and becomes yrast at $I = 41/2$. This crossing is between the $\alpha = -1/2$ states of the two bands, and the $\alpha = +1/2$ branch is quite high in excitation energy as compared with its signature partner band.

What is interesting to note from Fig. 1 is that, above the band crossing, the $\alpha = +1/2$ states of the yrast band originate from the γ band built on the three-quasiparticle state. In the TPSM analysis, γ bands are built on each quasiparticle state [43] and apart from the γ band based on the ground state, γ bands built on two-quasiparticle states have been identified in several even-even nuclei [32,37,55,56]. These bands have $K = K_0 + 2$, where K_0 is the K quantum number of the parent band. In the present work, the γ band based on the ground state, $K = 3/2$, has $K = 7/2$ and is located at an excitation energy of $\approx$1.0 MeV from the ground-state band at $I = 11/2$. The γ band built on the aligned three-quasiparticle state with $K = 1/2$ has $K = 5/2$ and is located at an excitation energy of $\approx$2.5 MeV at $I = 11/2$. This band is noted to cross the γ band based on the ground-state band at $I = 35/2$ and becomes the lowest band for $\alpha = +1/2$ signature branch. The reason that it becomes lowest is because it is built on the three-quasiparticle state with $K = 5/2$ and depicts less signature splitting as compared with its parent band. It is also noted

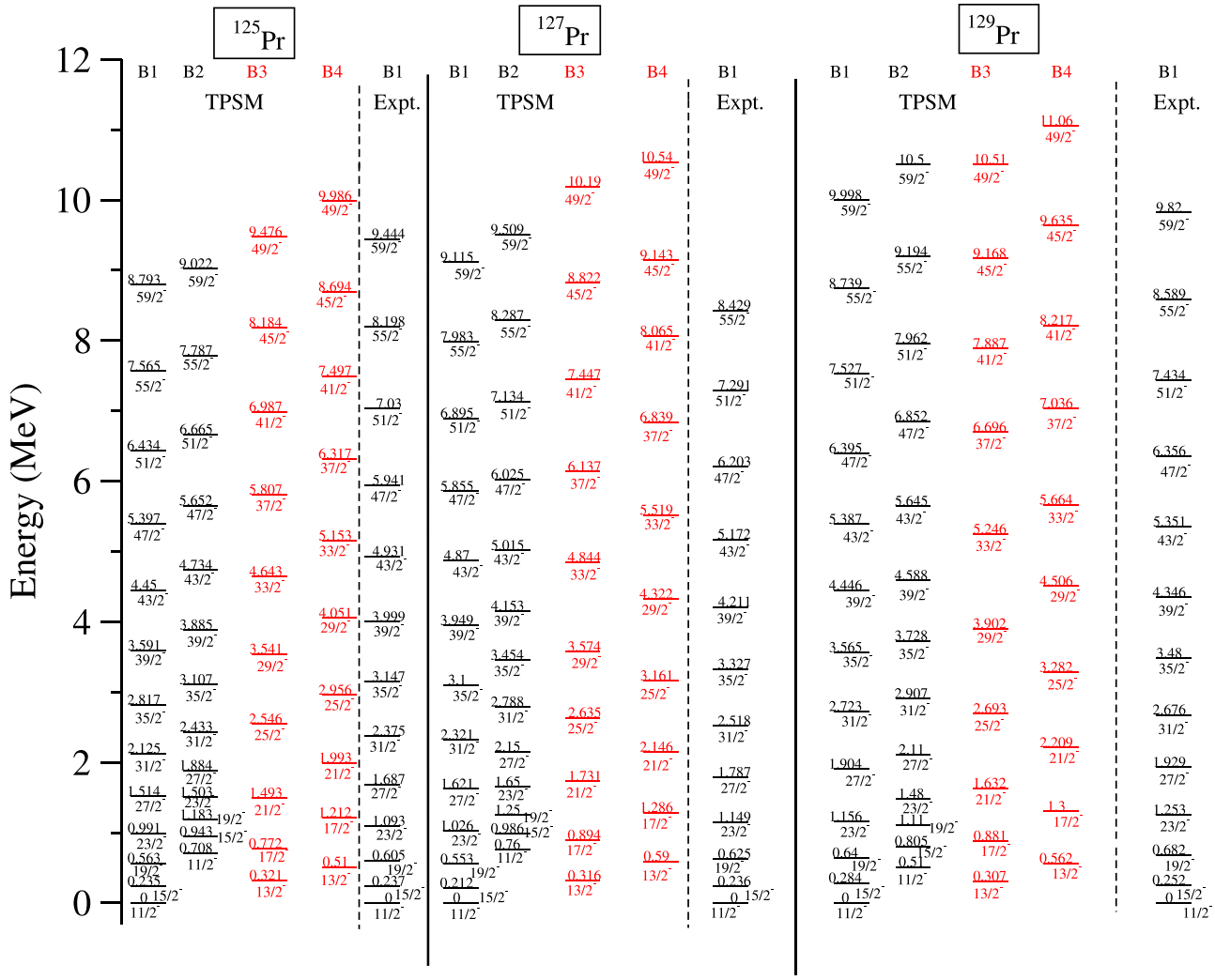

FIG. 9. TPSM energies for the lowest two bands after configuration mixing are plotted along with the available experimental data for ^{125,127,129}Pr isotopes. Data are taken from Ref. [38].

from Fig. 1 that a five-quasiparticle state, having both two protons and two neutrons aligned, with $K = 1/2$, crosses the three-quasiparticle state at a higher spin, $I = 59/2$.

The band diagrams for other studied Pr isotopes are similar to that of ^{125}Pr, except that nature of the band crossing changes with increasing neutron number. In Fig. 2, only the band crossing portion of the band diagrams is depicted for the praseodymium isotopes ranging from $A = 127$ to 137. The first band crossing in ^{127}Pr is again due to the alignment of two neutrons but occurs at $I = 39/2$, which is slightly lower compared with that of ^{125}Pr. For ^{129}Pr, the nature of the first band crossing has changed and is now due to the alignment of two-protons rather than of two-neutrons as was for the earlier two cases. The three-proton configuration having $K = 3/2$ becomes lower than one-quasiparticle ground-state band at $I = 35/2$. For ^{131}Pr, the band crossing occurs at $I = 35/2$ as for ^{129}Pr, but for other studied isotopes, it is observed at a higher angular-momentum of $I = 43/2$. These band-crossing features shall be discussed in detail later when comparing the alignment and moment of inertia obtained from the TPSM results with those deduced from the experimental data.

The band structures for ^{127}Pm are displayed in Fig. 3 and again only configurations important to describe the near-yrast spectroscopy are plotted. The ground-state band, having $K = 3/2$, is built on the one-quasiproton Nilsson state with energy of 0.93 MeV. The γ band based on the ground-state band, having $K = 7/2$ lies at an excitation energy of $\approx$1 MeV for $I = 11/2$. It is observed from the figure that three-quasiparticle state having $K = 1/2$ with one-proton coupled to two-aligned neutrons, crosses the ground-state band at $I = 43/2$. It is also noted from the figure that γ band built on the three-quasiparticle state, having $K = 5/2$, also crosses the ground-state band at $I = 47/2$. This almost simultaneous crossing will lead to forking of the ground-state band into two s bands as is known to occur in many even-even systems [33,37].

In the $A \approx 130$ region, some even-even isotopes of Ba, Ce, and Nd are known to have several s bands [33]. As the neutron and proton Fermi surfaces are close in energy for these isotopes, the forking of the ground-state band into two s bands is expected with one s band having neutron character and the other originating from protons. However, this traditional

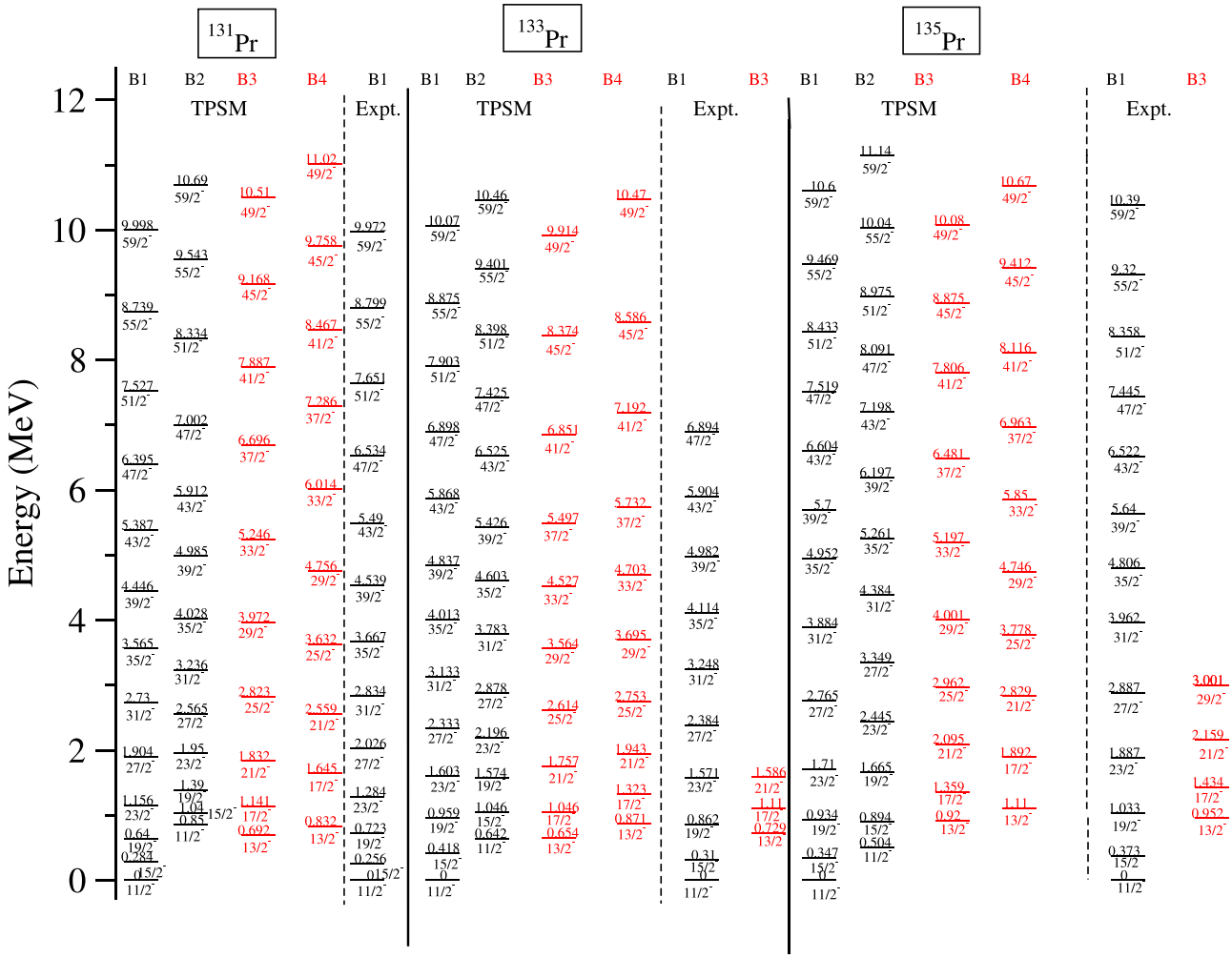

FIG. 10. TPSM energies for the lowest two bands after configuration mixing are plotted along with the available experimental data for $^{131-135}$Pr isotopes. Data are taken from Refs. [39,40].

picture cannot explain the magnetic moment measurements for the bandheads, $I = 10^+$ states, of the two s bands with g factors of both the states having a neutron character in ^{134}Ce [32]. This long-standing puzzle was addressed using the TPSM approach and it was shown [31] that the second s band in ^{134}Ce is a γ band based on the two-neutron-aligned state and since the intrinsic configurations of the two s bands are the same in this interpretation, the g factors of the two s bands are expected to be similar [37]. It was also predicted that two s bands observed in ^{136,138}Nd nuclei should both have positive g factors with the aligning particles being protons [37]. Furthermore, γ bands built on two-quasiparticle states have been observed in ^{70}Ge [56] and ^{156}Dy [55] nuclei.

In the present work, we examine whether it would be feasible to identify the γ bands built on quasiparticle states. γ bands in odd-mass nuclei are quite rare and these bands built on the ground state have been been identified in ^{103,105}Nb [44,57], ^{107,109}Tc [58], and, very recently, in ^{155,157}Dy nuclei [59]. The problem is that, in odd-mass nuclei, γ configurations compete with one-quasiparticle states and contain strong admixtures from these states. This shall be addressed later in the presentation of the bandhead energies of various band structures after diagonalization of the shell-model Hamiltonian.

The band diagrams for other studied Pm Isotopes are displayed in Fig. 4, depicting only the important band-crossing regions. The band crossing for ^{129}Pm and ^{131}Pm isotopes occur at $I = 39/2$ and is due to the alignment of two neutrons. For other Pr isotopes, the band crossing occurs at lower angular-momentum and is due to the alignment of two protons. It is also noted from Fig. 1 that the five-quasiparticle state, which contains three-proton plus two-neutron aligned configuration, crosses the three-quasiparticle state at higher angular momentum. Therefore, the present calculations predict that odd-Pm isotopes, studied in the present work, should depict a second crossing at high spin.

The angular-momentum projected states depicted in the band diagrams in Figs. 1–4 and many more in the vicinity of the Fermi surface are employed to diagonalize the shell-model Hamiltonian of Eq. (4). As already mentioned, that present approach is similar to the traditional spherical shell-model (SSM) approach with the exception that angular-momentum states, projected from the deformed Nilsson configurations, are employed as the basis states instead of the spherical

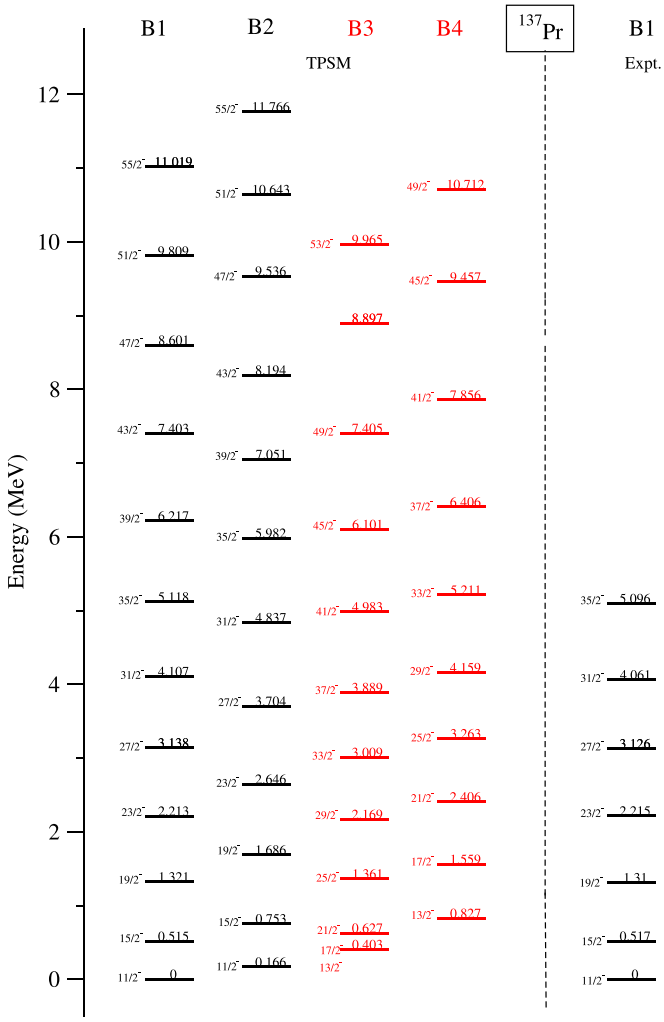

FIG. 11. TPSM energies for the lowest two bands after configuration mixing are plotted along with the available experimental data for ^{137}Pr isotope. Data are taken from Ref. [41].

configurations. The nuclei studied in the present work are beyond the reach of the SSM approach as the dimensionality of the spherical basis space becomes too prohibitive to manage with the existing computational facilities. In the TPSM approach, the optimal deformed basis states are chosen to describe the properties of deformed systems and the number of basis states required is quite minimal. In most of the studies, it has been demonstrated that 40 to 50 basis states are sufficient to describe the properties of deformed systems. The additional work required in the TPSM approach is that the deformed basis need to be projected onto states having good angular momentum in order to diagonalize the spherical shell-model Hamiltonian of Eq. (4).

In the studied Pr isotopes, the lowest projected states after diagonalization are depicted in Fig. 5 for the angular momentum, $I = 11/2$, which is the ground state for the negative-parity bands observed for the studied isotopes. The states in Fig. 5 are labeled with the projected intrinsic state that is most significant in the wave function. Note that ground-state for all the studied isotopes originates from the one-quasiparticle state having $K = 3/2$. The γ band based on the ground state, having $K = 7/2$, is located at about 1 MeV excitation energy from the ground state in all the isotopes. The main problem to identify them in odd-mass systems is that they are mixed with the single-particle states, as is evident from the figure that there are several single-quasiparticle states, which are in the vicinity of the γ bands. This figure also displays three-quasiparticle states and the γ bands built on them. These three-quasiparticle states become favored in energy at high spin and cross the ground-state band, as illustrated in the band diagrams in Figs. 1–4. It is also noted from Fig. 5 that these three-quasiparticle states become lower in energy for ^{135}Pr and ^{137}Pr isotopes and it might be feasible to populate the low-spin members of these states. In particular, the most interesting prediction is the possibility of observing almost two identical three-quasiparticle bands, one the normal three-quasiparticle band having $K = 1/2$ and the other the γ band, having $K = 5/2$, based on the three-quasiparticle state. These two states should have similar electromagnetic properties, like g factors, since they originate from the same intrinsic quasiparticle configuration.

The bandhead energies for the studied Pm isotopes are displayed in Fig. 6 and have a similar pattern as that for the Pr isotopes, shown in Fig. 5. The only difference between the two figures is that the bandhead energies for the three-quasiparticle band structures is slightly lower for the Pm isotopes. In particular, for ^{139}Pm, the three quasiparticle state and the γ band based on this state is quite low in energy and is the best candidate for which these structures could be identified in the future experimental studies.

The dominant components in the wave functions of the above-discussed bandhead states are depicted in Figs. 7 and 8 for $I = 11/2$. It is observed from these figures that all the states are mixed, even the ground-state bandhead has small admixtures from the other one-quasiparticle states and also from the γ band. We would like to remind the reader that projection from a triaxial intrinsic state give rise to several bands having different values of the K quantum number. The shell-model Hamiltonian is diagonalized with all these projected states that results in mixing among them. The γ band, which happens to be the first-excited band, also has mixing from the ground-state and other configurations. Although all the states are mixed, but it is possible to identify them at low-spin values because they have one predominant component. For high-spin states, the bands are highly mixed, and it is difficult to identify them.

The complete band structures for the lowest and the first-excited state, obtained after diagonalization of the shell model Hamiltonian, are depicted in Figs. 9–11 for Pr isotopes and in Figs. 12 and 13 for Pm isotopes and are compared with the experimental data, wherever available. For most of the nuclei, the ground-state band, except for ^{127}Pm and ^{129}Pm, are known up to quite high spin and the TPSM energies are noted to be in good agreement with these known level energies. Some preliminary TPSM results for ^{135}Pm were presented in the experimental work [16] and it was shown that the results agreed remarkably well with the data. The energy values for all the states have been specified in the Figs. 9–13, which shall be useful to make comparisons with future exper-

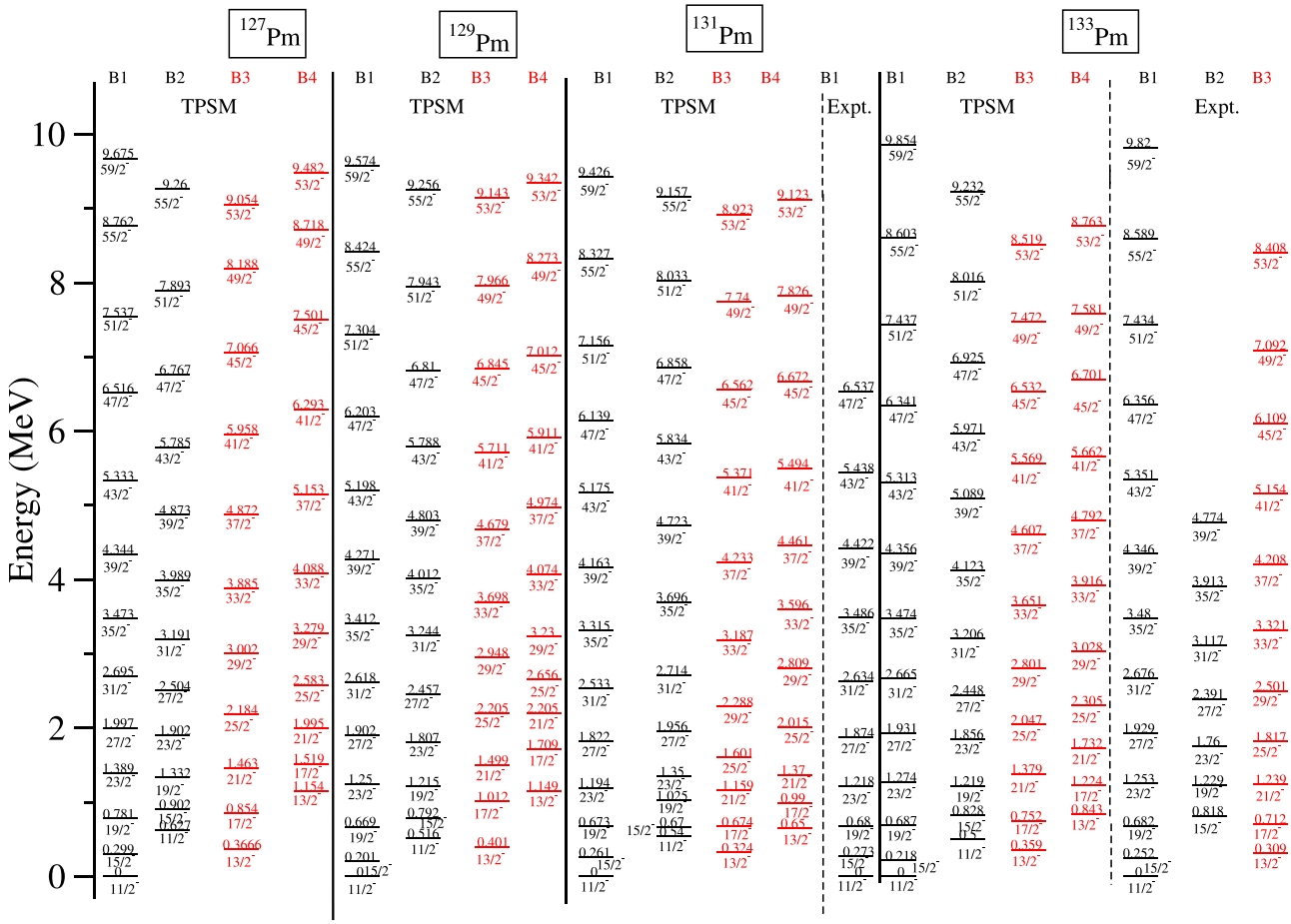

FIG. 12. TPSM energies for the lowest two bands after configuration mixing are plotted along with the available experimental data for $^{127-133}$Pm isotopes. Data are taken from Ref. [21].

imental measurements, and as well as with other theoretical studies.

We now turn our discussion to the band-crossing features observed in the studied Pr and Pm isotopes. As already stated in the introduction, the observed band crossing features in some of these isotopes could not be explained using the standard CSM approach and it was necessary to employ the self-consistent TRS approach to shed light on the anomalous band-crossing features. Furthermore, in the earlier PSM study of the odd-proton isotopes, only neutron-aligned states were considered in the basis space [22]. However, it was evident from the earlier analysis [21] that neutron and proton alignments compete, and it is imperative to include both two-neutron- and two-proton-aligned configurations in the basis space. In the present work, both these configurations have been included, and in the following we present the results of alignments and moments of inertia. Alignment, i_x and the dynamic moment of inertia $J^{(2)}$ have been evaluated using the standard expressions [60]. These quantities are displayed in Figs. 14 and 15 for the Pr isotopes. For ^{125}Pr, ^{127}Pr, and ^{129}Pr, both experimentally and TPSM-deduced i_x depict an increasing trend with spin and band crossing not evident from this plot. As we see below, $J^{(2)}$, which is more sensitive to changes in the alignment, depicts band-crossing features. i_x plots for ^{131}Pr, ^{133}Pr, ^{135}Pr, and ^{137}Pr show up-bends, which is indicative of a band crossing having large interaction strength between the ground-state and the aligned band. It is evident from the figure that TPSM results agree fairly well with those deduced from the experimental data.

For $^{125-133}$Pr isotopes, $J^{(2)}$ in Fig. 15 depict up-bends between spin values of $I = 31/2$ and $35/2$. The up-bend is a clear indication of the change in the configuration along the yrast band and is a signature of the band-crossing phenomenon. For ^{135}Pr, the up-bend in $J^{(2)}$ is noticed at a higher angular momenta of $I = 41/2$ and in the case of ^{137}Pr, and the discontinuity in $J^{(2)}$ is observed at a lower angular momentum. The $J^{(2)}$ evaluated from the measured energies depicts a larger enhancement as compared with the TPSM-predicted value.

For the isotopes of Pm from $A = 127$ to 135, i_x plotted in Fig. 16 depicts an increasing trend with spin. For $A = 127$ and 129, experimental quantities are not available, but for $A = 131$, 133, and 135, TPSM values are in good agreement with the data. For ^{137}Pm and ^{137}Pm, two up-bends are predicted by TPSM calculations, and for ^{139}Pm, both up-bends

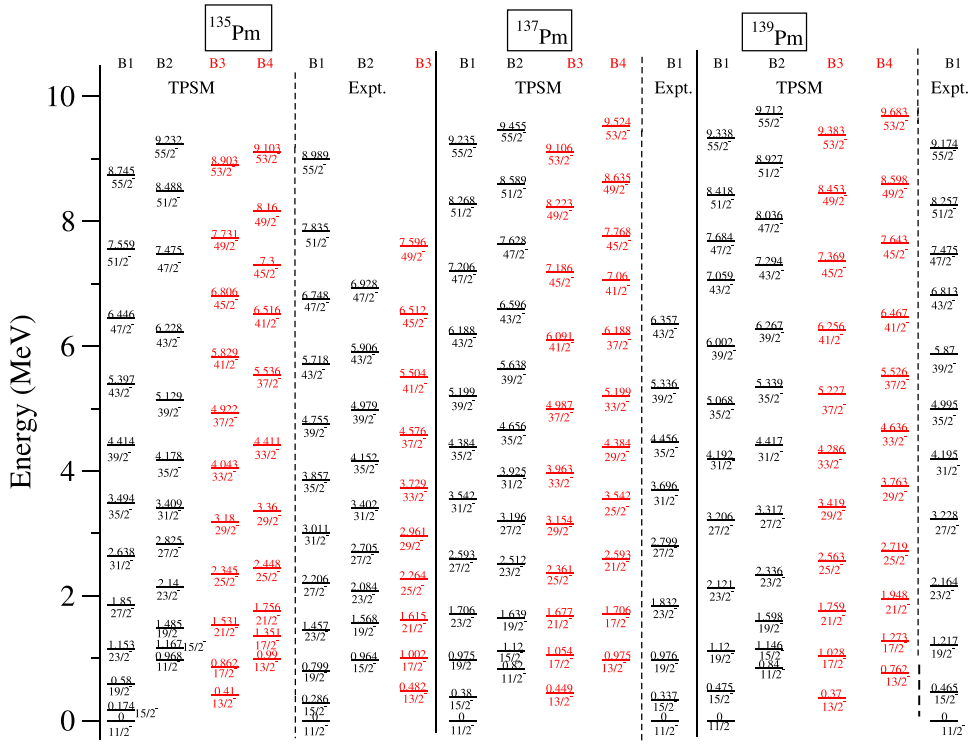

FIG. 13. TPSM energies for the lowest two bands after configuration mixing are plotted along with the available experimental data for $^{135-139}$Pm isotopes. Data are taken from Refs. [19,42].

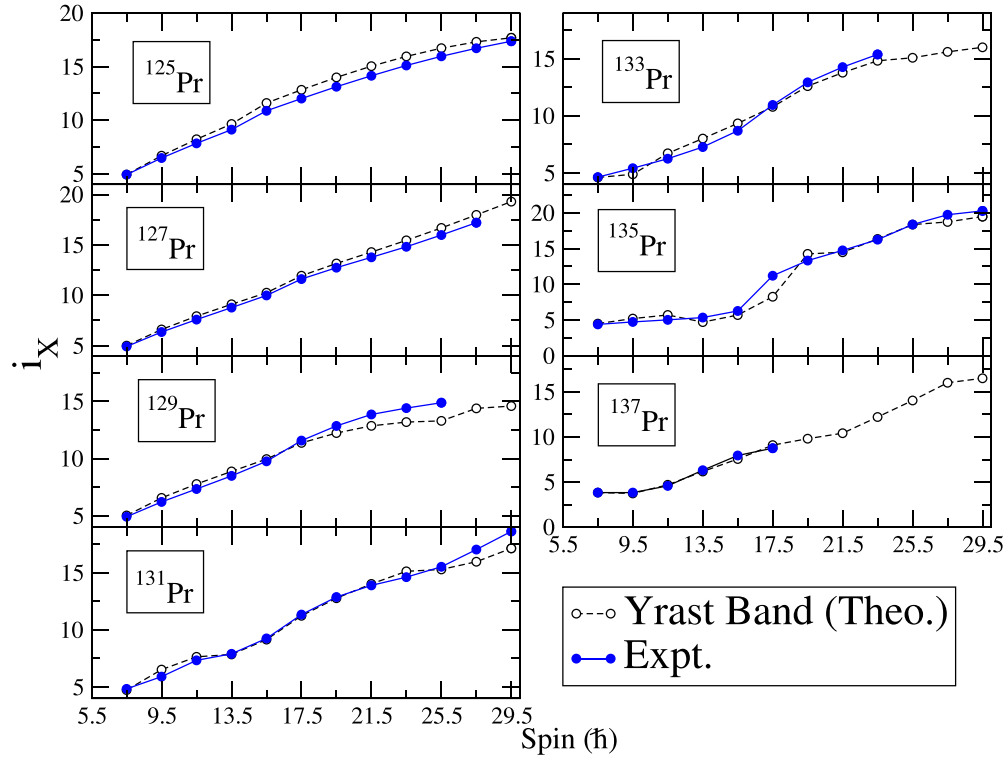

FIG. 14. Comparison of the aligned angular momentum, $i_x = I_x(\omega) - I_{x,\mathrm{ref}}(\omega)$, where $\hbar\omega = \frac{E_\gamma}{I_x^i(\omega) - I_x^f(\omega)}$, $I_x(\omega) = [I(I+1) - K^2]^{1/2}$ and $I_{x,\mathrm{ref}}(\omega) = \omega(J_0 + \omega^2 J_1)$. The reference band Harris parameters used are $J_0 = 23$ and $J_1 = 90$, obtained from the measured energy levels as well as those calculated from the TPSM results for $^{125-137}$Pr nuclei.

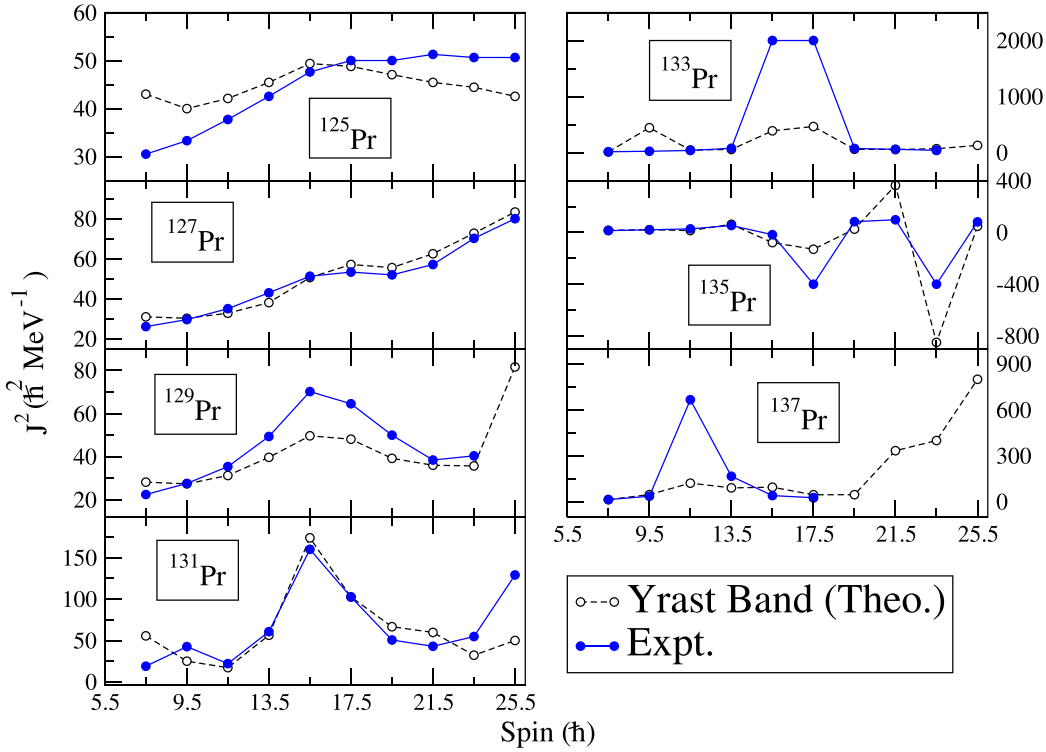

FIG. 15. Comparison between experimental and calculated dynamic moment of inertia, $J^{(2)} = \frac{4}{E_\gamma(I)-E_\gamma(I-2)}$, of the yrast band for $^{125-137}$Pr isotopes.

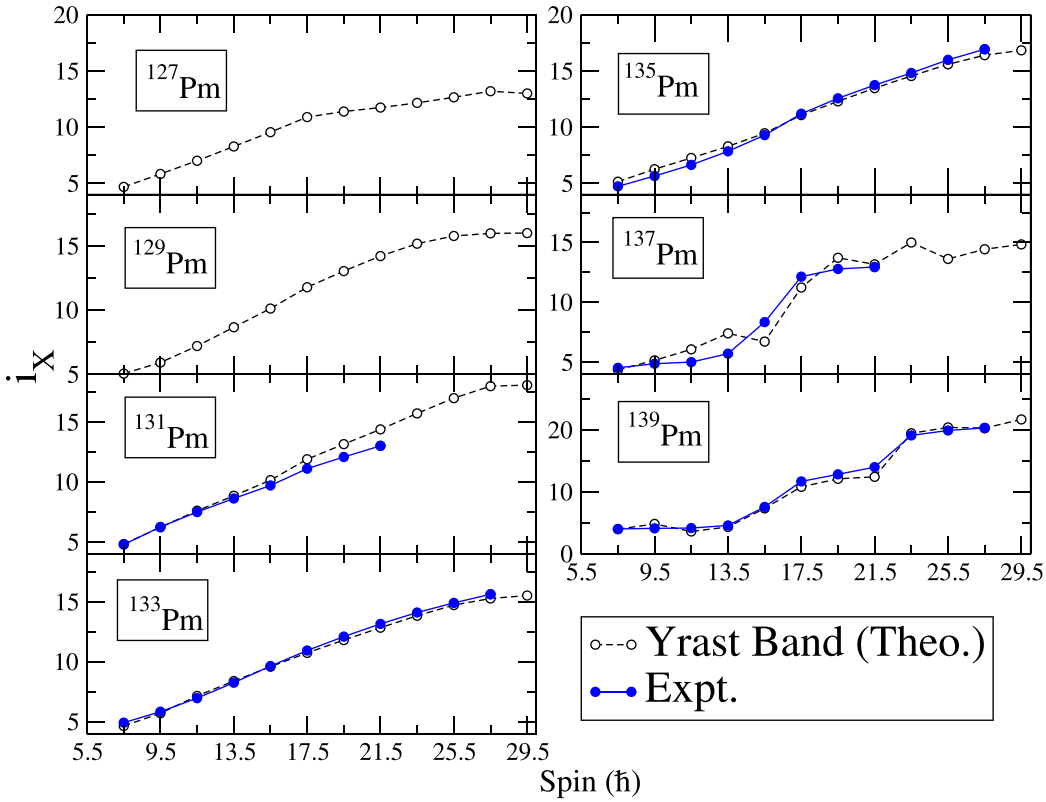

FIG. 16. Comparison of the measured and calculated aligned angular momentum (i_x) for $^{127-139}$Pm nuclei.

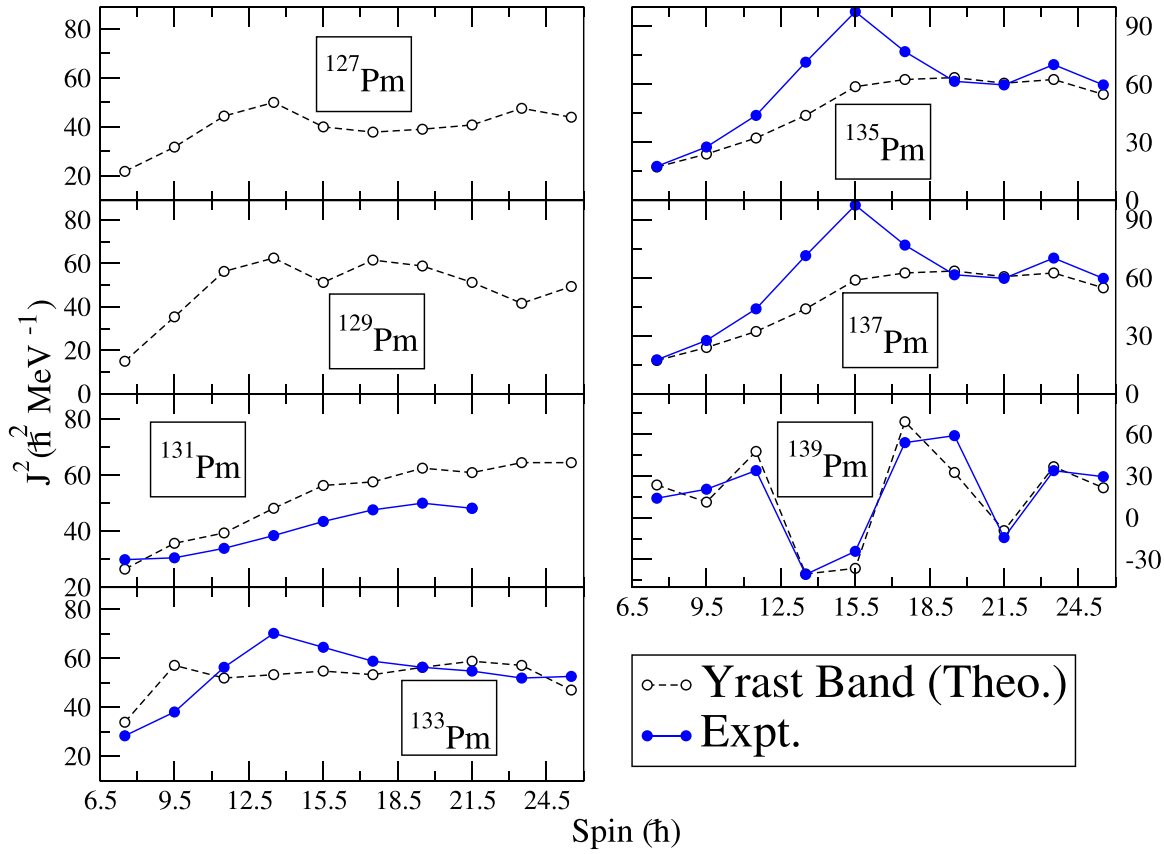

FIG. 17. Comparison between experimental and calculated dynamic moment of inertia ($J^{(2)}$) of the yrast band for $^{127-139}$Pm isotopes.

are observed in the experimental data. $J^{(2)}$ calculated for the studied Pm isotopes are depicted in Fig. 17 and are noted to be in good agreement with the known experimental quantities, except those for the isotopes of ^{135}Pm and ^{137}Pm, the TPSM-calculated up-bends are smoother than the experimental quantities.

It has been demonstrated using the self-consistent TRS model [21] that alignments for the studied odd-proton Pr and Pm isotopes are quite complicated, with considerable mixing between neutron and proton configurations. In the band diagrams of Figs. 2 and 4, the alignment is either due to protons or neutrons as the energies are plotted before configuration mixing. To investigate the mixing between the neutron and proton configurations, the wave function amplitudes are depicted in Fig. 18 for ^{127}Pr and ^{131}Pm, which were studied in detail in Ref. [21]. It is quite evident from the figure that band crossing is not entirely due to the alignment of two neutrons, but also has a significant contribution from the aligned proton configuration. For heavier isotopes, the situation is reversed with the proton contribution larger than the neutron contribution. Therefore, the present work substantiates the TRS prediction that alignments for odd-proton Pr and Pm isotopes are quite complicated with mixing between the proton- and neutron-aligned configurations. This is primarily because both aligned protons and neutrons occupy the same intruder orbital, $1h_{11/2}$.

IV. SUMMARY AND CONCLUSIONS

In the present work, the TPSM approach for odd-proton nuclei has been generalized to include three-proton and three-proton coupled to two-neutron quasiparticle configurations. This extension allows the application of the TPSM approach to high-spin band structures observed in odd-proton systems. In the earlier version, only one-proton and one-proton coupled to two-neutron configurations were considered, and this limited the application of the TPSM approach. In some odd-proton Pr and Pm isotopes, anomalous band-crossing features were reported using the standard CSM analysis. It was demonstrated, using a more realistic TRS approach in which pairing and deformation properties were obtained self-consistently, that the first band crossing in some Pr and Pm isotopes also contains a large contribution from the proton configuration. Normally, it is expected that, in odd-proton systems, the proton crossing is blocked for the yrast band and the first crossing is due to the alignment of two neutrons. It has been shown using the extended basis space that for lighter Pr and Pm isotopes, the band crossings is dominated by the alignment

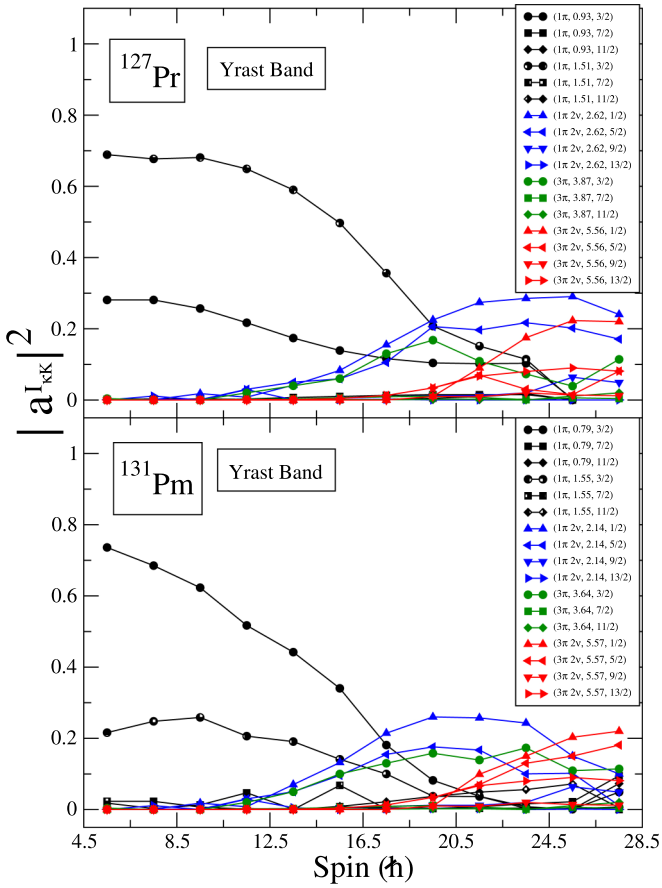

FIG. 18. Probability of various projected K-configurations in the wave functions of the yrast band after diagonalization for ^{127}Pr and ^{131}Pm isotopes

of neutrons. However, for heavier isotopes, it has been shown that first band crossing has a dominant contribution from the aligned protons. The present work also confirmed the TRS prediction that band crossings in Pr and Pm isotopes have mixed neutron- and proton-aligned configurations.

Furthermore, we have explored the possibility of observing γ bands in the studied odd-mass systems. γ bands are quite scarce in odd-mass systems and have been observed only in a few nuclei. In comparison, the γ bands in even-even systems have been observed, not only based on the ground state, but have also been identified built on two-quasiparticle excited configurations. In even-even Ce and Nd isotopes, several s bands are observed and it was shown that some of these s bands are, as a matter of fact, γ bands built on the two-quasiparticle states. Since Ce and Nd isotopes are even-even cores of Pr and Pm isotopes, it is expected that they should also depict some features of the even-even cores. It has been shown in the present work that heavier Pr and Pm isotopes are the best candidates to observe the γ bands based on three-quasiparticle configurations. We have provided the excitation energies of the bandheads of these structures, which shall be helpful for identifying them in future experimental studies.

ACKNOWLEDGMENTS

The authors would like to acknowledge the Science and Engineering Research Board (SERB), Department of Science and Technology (Govt. of India) for providing financial assistance under the Project No. CRG/2019/004960 to carry out a part of the present research work.

[1] K. Heyde and J. L. Wood, Rev. Mod. Phys. **83**, 1467 (2011).
[2] P. E. Garrett, J. Phys. G **43**, 084002 (2016).
[3] C. M. Parry, I. M. Hibbert, R. Wadsworth, A. N. Wilson, E. S. Paul, A. Galindo-Uribarri, V. P. Janzen, D. Ward, S. M. Mullins, P. H. Regan, C. E. Svensson, and R. Wyss, Phys. Rev. C **60**, 054314 (1999).
[4] D. T. Joss, E. S. Paul, D. E. Archer, M. Devlin, P. Fallon, I. M. Hibbert, D. R. LaFosse, P. J. Nolan, N. J. O'Brien, J. Pfohl, M. A. Riley, D. G. Sarantites, R. Sheline, J. Simpson, and R. Wadsworth, Phys. Rev. C **54**, R969(R) (1996).
[5] A. J. Kirwan, G. C. Ball, P. J. Bishop, M. J. Godfrey, P. J. Nolan, D. J. Thornley, D. J. G. Love, and A. H. Nelson, Phys. Rev. Lett. **58**, 467 (1987).
[6] K. Starosta, T. Koike, C. J. Chiara, D. B. Fossan, D. R. LaFosse, A. A. Hecht, C. W. Beausang, M. A. Caprio, J. R. Cooper, R. Krücken, J. R. Novak, N. V. Zamfir, K. E. Zyromski, D. J. Hartley, D. L. Balabanski, J. Zhang, S. Frauendorf, and V. I. Dimitrov, Phys. Rev. Lett. **86**, 971 (2001).
[7] A. J. Simons, P. Joshi, D. G. Jenkins, P. M. Raddon, R. Wadsworth, D. B. Fossan, T. Koike, C. Vaman, K. Starosta, E. S. Paul, H. J. Chantler, A. O. Evans, P. Bednarczyk, and D. Curien, J. Phys. G **31**, 541 (2005).
[8] S. Törmänen, S. Juutinen, R. Julin, B. Cederwall, A. Johnson, R. Wyss, P. Ahonen, B. Fant, M. Matsuzaki, J. Nyberg, M. Piiparinen, S. Mitarai, J. Mukai, and A. Virtanen, Nucl. Phys. A **572**, 417 (1994).
[9] J. M. Sears, D. B. Fossan, G. R. Gluckman, J. F. Smith, I. Thorslund, E. S. Paul, I. M. Hibbert, and R. Wadsworth, Phys. Rev. C **57**, 2991 (1998).
[10] R. Banik, S. Bhattacharyya, S. Biswas, S. Bhattacharya, G. Mukherjee, S. Rajbanshi, S. Dar, S. Nandi, S. Ali, S. Chatterjee, S. Das, S. D. Gupta, S. S. Ghugre, A. Goswami, A. Lemasson, D. Mondal, S. Mukhopadhyay, H. Pai, S. Pal, D. Pandit, R. Raut *et al.*, Phys. Rev. C **101**, 044306 (2020).
[11] A. Granderath, P. F. Mantica, R. Bengtsson, R. Wyss, P. von Brentano, A. Gelberg, and F. Seiffert, Nucl. Phys. A **597**, 427 (1996).
[12] C. M. Petrache, P. M. Walker, S. Guo, Q. B. Chen, S. Frauendorf, Y. X. Liu, R. A. Wyss, D. Mengoni, Y. H. Qiang, A. Astier, E. Dupont, R. Li, B. F. Lv, K. K. Zheng, D. Bazzacco, A. Boso, A. Goasduff, F. Recchia, D. Testov, F. Galtarossa *et al.*, Phys. Lett. B **795**, 241 (2019).
[13] X. L. Che, S. J. Zhu, M. L. Li, Y. J. Chen, Y. N. U, H. B. Ding, L. H. Zhu, X. G. Wu, G. S. Li, C. Y. He, and Y. Liu, Eur. Phys. J. A **30**, 347 (2006).

[14] S. J. Zhu, L. Y. Zhu, M. Li, C. Y. Gan, M. Sakhaee, L. M. Yang, R. Q. Xu, Z. Zhang, Z. Jiang, G. L. Long, S. X. Wen, X. G. Wu, and X. A. Liu, Phys. Rev. C **62**, 044310 (2000).
[15] Q. Xu, S. J. Zhu, X. L. Che, J. G. Wang, H. B. Ding, L. Gu, L. H. Zhu, X. G. Wu, Y. Liu, C. Y. He, and G. S. Li, Phys. Rev. C **78**, 034310 (2008).
[16] F. S. Babra, S. Jehangir, R. Palit, S. Biswas, B. Das, S. Rajbanshi, G. H. Bhat, J. A. Sheikh, B. Das, P. Dey, U. Garg, Md. S. R. Laskar, C. Palshetkar, S. Saha, L. P. Singh, and P. Singh, Phys. Rev. C **103**, 014316 (2021).
[17] A. N. Wilson, D. R. LaFosse, J. F. Smith, C. J. Chiara, A. J. Boston, M. P. Carpenter, H. J. Chantler, R. Charity, P. T. W. Choy, M. Devlin, A. M. Fletcher, D. B. Fossan, R. V. F. Janssens, D. G. Jenkins, N. S. Kelsall, F. G. Kondev, T. Koike, E. S. Paul, D. G. Sarantites, D. Seweryniak *et al.*, Phys. Rev. C **66**, 021305 (2002).
[18] E. S. Paul, C. Fox, A. J. Boston, H. J. Chantler, C. J. Chiara, R. M. Clark, M. Cromaz, M. Descovich, P. Fallon, D. B. Fossan, A. A. Hecht, T. Koike, I. Y. Lee, A. O. Macchiavelli, P. J. Nolan, K. Starosta, R. Wadsworth, and I. Ragnarsson, Phys. Rev. C **84**, 047302 (2011).
[19] A. Dhal, R. K. Sinha, D. Negi, T. Trivedi, M. K. Raju, D. Choudhury, G. Mohanto, S. Kumar, J. Gehlot, R. Kumar, S. Nath, S. S. Ghugre, R. P. Singh, J. J. Das, S. Muralithar, N. Madhavan, J. B. Gupta, A. K. Sinha, A. K. Jain, I. M. Govil *et al.*, Eur. Phys. J. A **48**, 28 (2012).
[20] T. B. Brown, J. Pfohl, M. A. Riley, D. J. Hartley, D. G. Sarantites, M. Devlin, D. R. LaFosse, F. Lerma, D. E. Archer, R. M. Clark, P. Fallon, I. M. Hibbert, D. T. Joss, P. J. Nolan, N. J. O'Brien, E. S. Paul, R. K. Sheline, J. Simpson, R. Wadsworth, and Y. Sun, Phys. Rev. C **56**, R1210 (1997).
[21] C. M. Parry, A. J. Boston, C. Chandler, A. Galindo-Uribarri, I. M. Hibbert, V. P. Janzen, D. T. Joss, S. M. Mullins, P. J. Nolan, E. S. Paul, P. H. Regan, S. M. Vincent, R. Wadsworth, D. Ward, and R. Wyss, Phys. Rev. C **57**, 2215 (1998).
[22] A. Ibáñez-Sandoval, M. E. Ortiz, V. Velázquez, A. Galindo-Uribarri, P. O. Hess, and Y. Sun, Phys. Rev. C **83**, 034308 (2011).
[23] L.-J. Wang, F.-Q. Chen, T. Mizusaki, M. Oi, and Y. Sun, Phys. Rev. C **90**, 011303 (2014).
[24] L.-J. Wang, Y. Sun, T. Mizusaki, M. Oi, and S. K. Ghorui, Phys. Rev. C **93**, 034322 (2016).
[25] L.-J. Wang, Y. Sun, and S. K. Ghorui, Phys. Rev. C **97**, 044302 (2018).
[26] G. H. Bhat, J. A. Sheikh, W. A. Dar, S. Jehangir, R. Palit, and P. A. Ganai, Phys. Lett. B **738**, 218 (2014).
[27] A. Navin, M. Rejmund, S. Bhattacharyya, R. Palit, G. H. Bhat, J. A. Sheikh, A. Lemasson, S. Bhattacharya, M. Caamaño, E. Clément, O. Delaune, F. Farget, G. de France, and B. Jacquot, Phys. Lett. B **767**, 480 (2017).
[28] S. Biswas, R. Palit, U. Garg, G. H. Bhat, S. Frauendorf, W. Li, J. A. Sheikh, J. Sethi, S. Saha, P. Singh, D. Choudhury, J. T. Matta, A. D. Ayangeakaa, W. A. Dar, V. Singh, and S. Sihotra, Eur. Phys. J. A **55**, 159 (2019).
[29] V. Singh, S. Sihotra, G. H. Bhat, J. A. Sheikh, M. Kaur, S. Kumar, K. Singh, J. Goswamy, S. Saha, J. Sethi, R. Palit, S. S. Malik, N. Singh, U. Garg, and D. Mehta, Phys. Rev. C **95**, 064312 (2017).
[30] G. H. Bhat, J. A. Sheikh, and R. Palit, Phys. Lett. B **707**, 250 (2012).
[31] J. A. Sheikh, G. H. Bhat, R. Palit, Z. Naik, and Y. Sun, Nucl. Phys. A **824**, 58 (2009).
[32] A. Zemel, C. Broude, E. Dafni, A. Gelberg, M. B. Goldberg, J. Gerber, G. J. Kumbartzki, and K.-H. Speidel, Nucl. Phys. A **383**, 165 (1982).
[33] R. Wyss, A. Granderath, R. Bengtsson, P. von Brentano, A. Dewald, A. Gelberg, A. Gizon, J. Gizon, S. Harissopulos, A. Johnson, W. Lieberz, W. Nazarewicz, J. Nyberg, and K. Schiffer, Nucl. Phys. A **505**, 337 (1989).
[34] K. Schiffer, A. Dewald, A. Gelberg, R. Reinhardt, K. O. Zell, Sun Xianfu, and P. von Brentano, Z. Phys. A **327**, 251 (1987).
[35] R. Wyss, J. Nyberg, A. Johnson, R. Bengtsson, and W. Nazarewicz, Z. Phys. A **329**, 255 (1988).
[36] R. Wyss, J. Nyberg, A. Johnson, R. Bengtsson, and W. Nazarewicz, Phys. Lett. B **215**, 211 (1988).
[37] S. Jehangir, G. H. Bhat, J. A. Sheikh, R. Palit, and P. A. Ganai, Nucl. Phys. A **968**, 48 (2017).
[38] P. K. Weng, P. F. Hua, S. G. Li, S. X. Wen, L. H. Zhu, L. K. Zhang, G. J. Yuan, G. S. Li, P. S. Yu, C. X. Yang, X. F. Sun, Y. X. Guo, and X. G. Lei, Phys. Rev. C **47**, 1428 (1993).
[39] L. Hildingsson, C. W. Beausang, D. B. Fossan, and W. F. Piel, Phys. Rev. C **33**, 2200(R) (1986).
[40] S. Botelho, W. A. Seale, L. G. R. Emediato, J. R. B. Oliveira, M. N. Rao, R. V. Ribas, N. H. Medina, E. W. Cybulska, M. A. Rizzutto, and F. R. Espinoza-Quiñones, G. García-Bermúdez, H. Somacal, and M. A. Cardona, Phys. Rev. C **58**, 3726 (1998).
[41] N. Xu, C. W. Beausang, R. Ma, E. S. Paul, W. F. Piel, Jr., D. B. Fossan, and L. Hildiggsson, Phys. Rev. C **39**, 1799 (1989).
[42] N. T. Zhang, Y. H. Zhang, X. H. Zhou, M. L. Liu, Y. Zheng, J. G. Wang, Y. D. Fang, B. Ding, W. J. Huang, Y. X. Guo, X. G. Lei, L. Chen, S. T. Wang, X. G. Wu, and Y. Zheng, Phys. Rev. C **84**, 057302 (2011).
[43] J. A. Sheikh, G. H. Bhat, W. A. Dar, S. Jehangir, and P. A. Ganai, Phys. Scr. **91**, 063015 (2016).
[44] J. A. Sheikh, G. H. Bhat, Y. Sun, and R. Palit, Phys. Lett. B **688**, 305 (2010).
[45] S. Jehangir, G. H. Bhat, J. A. Sheikh, S. Frauendorf, S. N. T. Majola, P. A. Ganai, and J. F. Sharpey-Schafer, Phys. Rev. C **97**, 014310 (2018).
[46] P. Ring and P. Schuck, *The Nuclear Many-Body Problem* (Springer-Verlag, New York, 1980).
[47] K. Kumar and M. Baranger, Nucl. Phys. A **122**, 273 (1968).
[48] S. G. Nilsson, C. F. Tsang, A. Sobiczewski, Z. Szymanski, S. Wycech, C. Gustafson, I. Lamm, P. Moller, and B. Nilsson, Nucl. Phys. A **131**, 1 (1969).
[49] K. Hara and Y. Sun, Int. J. Mod. Phys. E **4**, 637 (1995).
[50] Y. Sun, Phys. Scr. **91**, 043005 (2016).
[51] D. L. Hill and J. A. Wheeler, Phys. Rev. **89**, 1102 (1953).
[52] P. Möller and J. R. Nix, At. Data Nucl. Data Tables **59**, 185 (1995).
[53] H. A. Lamme and E. Boeker, Nucl. Phys. A **111**, 492 (1968).
[54] H. A. Lamme and E. Boeker, Nucl. Phys. A **136**, 609 (1969).
[55] S. N. T. Majola, D. J. Hartley, L. L. Riedinger, J. F. Sharpey-Schafer, J. M. Allmond, C. Beausang, M. P. Carpenter, C. J. Chiara, N. Cooper, D. Curien, B. J. P. Gall, P. E. Garrett, R. V. F. Janssens, F. G. Kondev, W. D. Kulp, T. Lauritsen, E. A. McCutchan, D. Miller, J. Piot, N. Redon *et al.*, Phys. Rev. C **91**, 034330 (2015).
[56] M. Kumar Raju, P. V. Madhusudhana Rao, S. Muralithar, R. P. Singh, G. H. Bhat, J. A. Sheikh, S. K. Tandel, P. Sugathan,

T. Seshi Reddy, B. V. Thirumala Rao, and R. K. Bhowmik, Phys. Rev. C **93**, 034317 (2016).

[57] H. J. Li, S. J. Zhu, J. H. Hamilton, A. V. Ramayya, J. K. Hwang, Y. X. Liu, Y. Sun, Z. G. Xiao, E. H. Wang, J. M. Eldridge, Z. Zhang, J. O. Rasmussen, I. Y. Lee, G. M. Ter-Akopian, A. V. Daniel, Yu. Ts. Oganessian, and W. C. Ma, Phys. Rev. C **88**, 054311 (2013).

[58] G. Long, Z. Sheng-Jiang, J. H. Hamilton, A. V. Ramayya, J. K. Hwang, S. H. Liu, W. Jian-Guo, Y. X. Luo, J. O. Rasmussen, I. Y. Lee, X. Qiang, E. Y. Yeoh, and W. C. Ma, Chin. Phys. Lett. **27**, 062501 (2010).

[59] S. N. T. Majola, M. A. Sithole, L. Mdletshe, D. Hartley, J. Timár, B. M. Nyakó, J. M. Allmond, R. A. Bark, C. Beausang, L. Bianco, T. D. Bucher, S. P. Bvumbi, M. P. Carpenter, C. J. Chiara, N. Cooper, D. M. Cullen, D. Curien, T. S. Dinoko, B. J. P. Gall, P. E. Garrett *et al.*, Phys. Rev. C **101**, 044312 (2020).

[60] R. Bengtsson and S. Frauendorf, Nucl. Phys. A **314**, 27 (1979).